17th Brazilian Congress of Thermal Sciences and Engineering
November 25th-28th, 2018, Águas de Lindóia, SP, Brazil

ENCIT-2018
NUMERIC SIMULATION OF TURBULENT FLOW DEVELOPMENT IN AN ECCENTRIC CHANNEL WITH CONVECTIVE HEAT TRANSFER

Diana Caterinne Sandoval Candela
Jhon Nero Vaz Goulart
University of Brasilia, Gama, 72.405-610, Brazil
Diana.csandovalc@gmail.com
Jvaz@unb.br
Thiago Ferreira Gomes
University of Brasilia, Gama, 72.405-610, Brazil
Fgomes.thiago@gmail.com

Abstract. *Non-isothermal numerical analysis of developing turbulent flow in an eccentric annular channel with outer-diameter, Do = 50.80 mm, Di/Do-ratio of 0.5 and an eccentricity, e = 0.8 was performed. Prescribed heat flux of 100 [W/m^2] was imposed at the inner wall tube, along with insulated boundary condition at outer wall tube. The flow has a Reynolds number of 7300 and a Prandtl number of 0.7. To model the additional diffusion caused by the turbulence, the DES-SST model was employed. Such model solves the flow field switching to LES simulation wherever is possible and k-w SST model in the other regions. The geometry of the problem presented in this work matches with the one used by Choueiri and Tavoularis in their experimental work in the 2014 allowing to validate the dynamics of the flow. A concentric case was also simulated and compared with the analytical equations presented by Gnielinski in his work in 2011. Such work was used as a source of validation of the methodology used for the eccentric case. It was found that the model used were successful in predicting the characteristics of the flow. Quase-peridic flow patterns were found at the gap vicinity and as well as the experimental results, the onset gap instabilities started around x/Dh =30 for all the measurements points. The Nusselt number as was expected, presented a behavior related with the velocity fluctuations, starting to fluctuate around a stable value at the same point as the velocities.*

Keywords: *turbulent flow, eccentric channel, convective, heat transfer, incompressible flow, DES-SST model, Nusselt number*

1. INTRODUCTION

Many mechanical systems used in industrial applications are constituted by a simple stationary annulus with fluid passing through the gap between inner and outer cylindrical walls, for instance, heat, exchangers, electrical motors and generators, cores of nuclear reactors and more. In many cases, the design tolerances and manufacturing limits can cause a misalignment in the inner and outer wall, creating an eccentricity between the two cylinders. This is reason the eccentric annulus and the non-circular passages have become of interest to researches in recent years.

As in the case of just purely dynamics of the flow, the concentric cases with laminar flow have been more developed and studied than non-circular passages and eccentric annuli with heat transfer. In 1963, Reynolds et al. (1963) presented the solution for the problem of heat transfer in fully developed laminar flow in concentric annulus. In the same field, Gnielinski (2011) presented analytical equations to obtain the friction factor and Nusselt number in concentric annuli taking into account the geometry of the problem, the Reynolds number and the characteristics of the heat transfer. Such work gives specific constants to be used depending of the thermal boundary conditions of the. For the case of eccentric channels and other non-circular passages, there are some studies developed, however, not so much extent compared with the concentric case. Studies performed in eccentric case, with different Reynolds numbers, radius ratio and thermal boundary conditions, have shown that the effect of increasing eccentricity generally leads to a decrease of Nusselt number compared with the concentric case with the same geometrical and thermal conditions *e.g*. Deissler *et al.*, 1955; Kays *et al.*,1963; Judd *et al.*, 1963; Ogino *et al.*, 1987. Recent studies have been conducted using also vertical flow developing in eccentric annuli passage, in these cases was found that, unlike the horizontal arrangement, the rate of heat transfer increases with the increase of the eccentricity ratio and is higher compared with the concentric and circular pipe cases (Hosseini *et al.*, 2009). Besides the forced convection, the free convection and mixed convection heat transfer was also studied by several authors through experimental and numerical computations. It was found, that in most, the horizontal forced convection, the Nusselt number and Raleigh number presented a decrease with the increase of the eccentricity (Kuehn *et al.*, 1978; Teamah *et al.*, 2000; Djezzar *et al.*, 2005; Kassem, 2007).

This works aims to perform a numeric simulation of a turbulent flow in an eccentric annulus using a commercial plataform. The computational domain was the same proposed by Choueiri and Tavoularis in his work of 2014. It was

added a convective heat transfer problem in order to validate the influence of the gap instabilities in the heat transfer coefficient and therefore the Nusselt number. The model used for the simulation was the hybrid turbulence model known as Detached Eddy Simulation (DES) with and advection scheme of Bounded Central Differences (BCD).

2. COMPUTATIONAL DOMAIN AND NUMERICAL METHODOLOGY

All the simulations were made in a computational domain with the same geometric parameters used by Choueiri and Tavoularis (Choueiri and Tavoularis, 2014) in their experimental work. The domain consist of an external tube with a diameter of 50.8 mm and an internal tube with 25.1 mm of diameter, giving a diameter ratio *Di/Do* of 0,5 approximately and a hydraulic diameter D_h of 25.7 mm. The tube presents an eccentricity *e* of 0.8 and a total length of 1500 mm as shown in Fig. 1. The equations of the eccentricity and the hydraulic diameter are presented in the Eq. (1) and Eq. (2) respectively.

The origin of the Cartesian coordinates is located in the center of the outer diameter and in the beginning of the channel, with the flow flowing in the *x* direction, from the left to the right of the Fig. 1(a). The spanwise direction of the flow coincides with de *z* axis and the *y* axis points towards the streamwise direction.

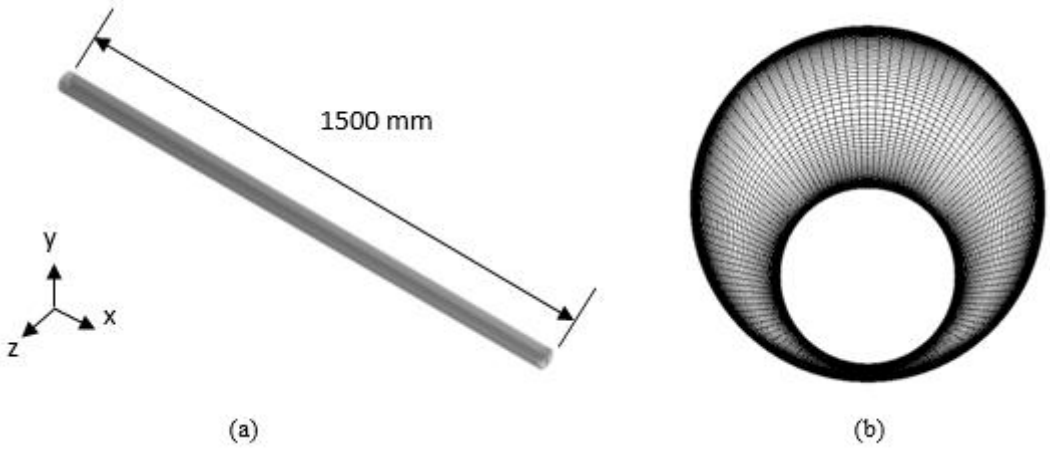

Figure 1. Computational domain. (a) Schematic view of the channel. (b) Cross-section of the channel.

$$e = \frac{2\Delta y}{D_o - D_i} \tag{1}$$

$$D_h = D_o - D_i \tag{2}$$

During the simulation, the time step used was $1.5*10^{-4}$ s, which allowed maintaining a Courant number lower than one during the 3 seconds of simulation that corresponded to approximately 9 flow-through times. A Hybrid Detached Eddy Simulation (*DES*) was used to model the turbulent flow in the channel described above. The DES-SST model has the ability to switch between LES and *k-ω SST* formulations, away from the walls and near the walls, respectively.

The present simulation uses air as work flow, the air is modeled as an incompressible flow for which the Navier stokes equations of continuity and momentum and energy are:

$\frac{\partial \overline{u_i}}{\partial x_i} = 0$	(3)
$\frac{\partial \overline{u}}{\partial t} + \frac{\partial \left(\overline{u_i u_j}\right)}{\partial x_j} = -\frac{1}{\rho}\frac{\partial \overline{P}}{\partial x_i} + \upsilon \frac{\partial^2 \overline{u_i}}{\partial x_j^2} + \frac{\partial \tau_{ij}}{\partial x_j}$	(4)
$\frac{D\theta}{Dt} = \kappa \nabla^2 \theta - \left(\frac{\partial}{\partial x}\overline{u'\theta'} + \frac{\partial}{\partial y}\overline{v'\theta'} + \frac{\partial}{\partial z}\overline{w'\theta'} \right)$	(5)

Taking into account that in this work was applied a hybrid model, it is important to clarify that some values of the Eq. (4) has different interpretations in each one of the sub-models used in this simulation. For the case of the regions that respond to the URANS model that correspond to the *k-w* SST model, the overbar represents the time average of the quantity and the τ_{ij} represents the Reynolds stress tensor. On the other hand, for the regions that LES model is applied, the overbar indicates a spatial averaging which gives a filtered variable. The τ_{ij} represents the sub-grid scale stress

tensor (*SGS stress tensor*) that can determine the dynamical coupling between large and small scales in turbulence and unlike Reynolds stress tensor, is a fluctuating turbulence quantity. Equations (6) and (7) presents the calculation of τ_{ij} for the Reynolds stress tensor where $\bar{S}_{ij}$ represents the strain rate tensor and Eq. (8) shows the SGS stress tensor. The double over bar term in Eq. (8) can be computed with the difference between the average instantaneous velocities correlation and the average of the instantaneous velocities.

$$\tau_{ij} = 2\mu_t \bar{S}_{ij} - \frac{2}{3}\delta_{ij}\rho k \tag{6}$$

$$\bar{S}_{ij} = \frac{1}{2}\left(\frac{\partial \overline{u_i}}{\partial x_j} + \frac{\partial \overline{v_j}}{\partial x_i}\right) \tag{7}$$

$$\tau_{ij} = \rho\overline{u_i u_j} - \rho\overline{\bar{u}_i \bar{u}_j} \tag{8}$$

The DES model combines features of RANS with characteristics of LES formulations; it was proposed by Spalart Allmaras. DES model is based in the idea of using RANS in attached and mildly separated boundary layers and switching to the use of LES in massively separated regions. The switching between de regions solved with RANS and the ones solved with LES model is made using the idea of the DES model proposed by Strelets (Strelets, 2001). The main idea is to switch between the regions where the turbulent length L_t is lower than the local grid spacing, in these cases the RANS model is used, otherwise, the LES model is activated. The magnitude of L_t is calculated in terms of the turbulent kinetic energy k and the turbulent eddy frequency ω as presented in Eq. (9). It is important to notice that in the cases where the LES model is activated, the quantity L_t is replaced by $C_{DES}\Delta_{max}$, where Δ_{max} is the maximum edge size of the computational domain in any direction.

$$\beta^* k\omega = \frac{k^{\frac{3}{2}}}{L_t} \rightarrow L_t = \frac{\sqrt{k}}{\beta^* \omega} \tag{9}$$

The Strelets (Strelets, 2001) modification is formulated as a multiplier to the destruction term of the turbulent kinetic energy equation k, where ε represents the turbulence eddy dissipation and F_{DES} is the switching function.

$$\varepsilon = \beta^* k\omega F_{DES} \tag{10}$$

$$F_{DES} = max\left(\frac{L_t}{C_{DES}\Delta}, 1\right) \rightarrow C_{DES} = 0{,}61 \tag{11}$$

For ANSYS® - CFX exist the option of a zonal formulation of the DES model based on the blending functions of the SST model as shown in Eq. (12). When F_{SST} is setted as zero, the Strelets model is applied (Strelets, 2001). That was the case used for this simulation.

$$F_{DES-CFX} = max\left(\frac{L_t}{C_{DES}\Delta}\left(1 - F_{SST}\right), 1\right) \rightarrow F_{SST} = 0, F_1, F_2 \tag{12}$$

The mesh in the transversal section was built in order to assure near the walls a size small enough to capture the behavior of the different regions that occur when the distance from the wall is increasing; the value of y+ used near the inner and outer wall was 0.22. In the stream wise direction of the domain 300 equidistant points were used, which produced a cell size of 6 mm and it was taking into account that the bigger cell in de transversal section were smaller than the cells in stream wise direction

All the results presented in the next section were taken in five points of the cross-plane as shown in the Fig. 2, now and forwards it is important to remember that the streamwise and spanwise directions coincides with the $\boldsymbol{x}$ and $\boldsymbol{z}$ axis. The Table 1 presents the $\boldsymbol{z}$ and $\boldsymbol{y}$ coordinates of each point.

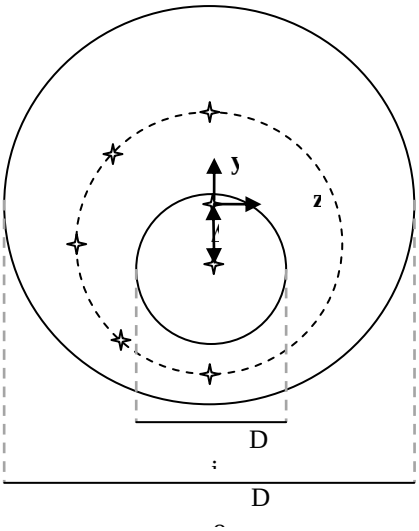

Figure 2. Points of measurement in the cross section.

Table 1. Coordinates of the measurement points

Point	*Z*	*Y*
1	0	-0.024384
2	0.013716	-0.018796
3	0.019304	-0.00508
4	0.013716	0.008636
5	0	0.014224

3. RESULTS

The results that are going to be presented in this section correspond to a four diferent cases:

1. Eccentric case without heat transfer
2. Concentric case without heat transfer
3. Eccentric case with heat transfer (inner wall with constant flux 100 [W/m^2], outer wall insulated)
4. Concentric case with heat transfer (inner wall with constant flux 100 [W/m^2] , outer wall insulated)

The first case will be validated with the experimental results of the work of Choueiri (Choueiri and Tavoularis, 2014) and compared with the concentric case in order to know some effects of the eccentricity of the geometry. The third case will be compared with the concentric case, the last one being validated with the analytic equations given by Gnielinski (Gnielinski, 2011).

3.1 Mean flow development

In order to validate the velocity field along the eccentric channel, measurements of the three components velocities and its respective mean values were taken at the five positions presented in Fig. 2. The development of the velocities are presented in Fig. 3. It is possible to see in the cases of the spanwise velocity who matches with the $\boldsymbol{z}$ axis and the $\boldsymbol{v}$ velocity, that the ratio between the local velocity and bulk velocity fluctuates around 0 independent of the measurement point. Besides that, the beginning of the fluctuation is more or less at $^{x}/_{D_h} = 30$ for the spanwise direction. For the streamwise velocity, it is possible to see two kinds of behavior. At the points 1 and 2 at the beginning of the channel is reached a peak of velocity of around $1.2U_b$. From this point to $^{x}/_{D_h} = 20$ the ratio of velocities decrease to $0.15U_b$ in point 1 and $0.6U_b$ in the point 2. From $20 < {}^{x}/_{D_h} < 40$ there is an increase of the mean velocity and the fluctuations start to appear around $^{x}/_{D_h} = 30$ and from this zone, is possible to see the establishment of the mean velocities and fluctuations. For the points 3, 4 and 5, the pattern in the first two regions it is different from the points 1 and 2. Unlike

the first two cases, from $0 < {}^{x}/_{D_h} < 20$ there is an increase of the mean velocity. However, the point 3 reach the maximum sooner that points 4 and 5 and start a decrease that continues in the next region before the establishment of the mean value and the fluctuations. The three regions mentioned above and the behavior presented in each point for velocity, matches with the experimental results encountered by Choueiri (Choueiri and Tavoularis, 2014). They defined this regions as entrance region from $0 < {}^{x}/_{D_h} < 20$, fluctuations growth region $20 < {}^{x}/_{D_h} < 40$ and rapid mixing region $40 < {}^{x}/_{D_h} < 60$. These definitions are going to be used in the present work.

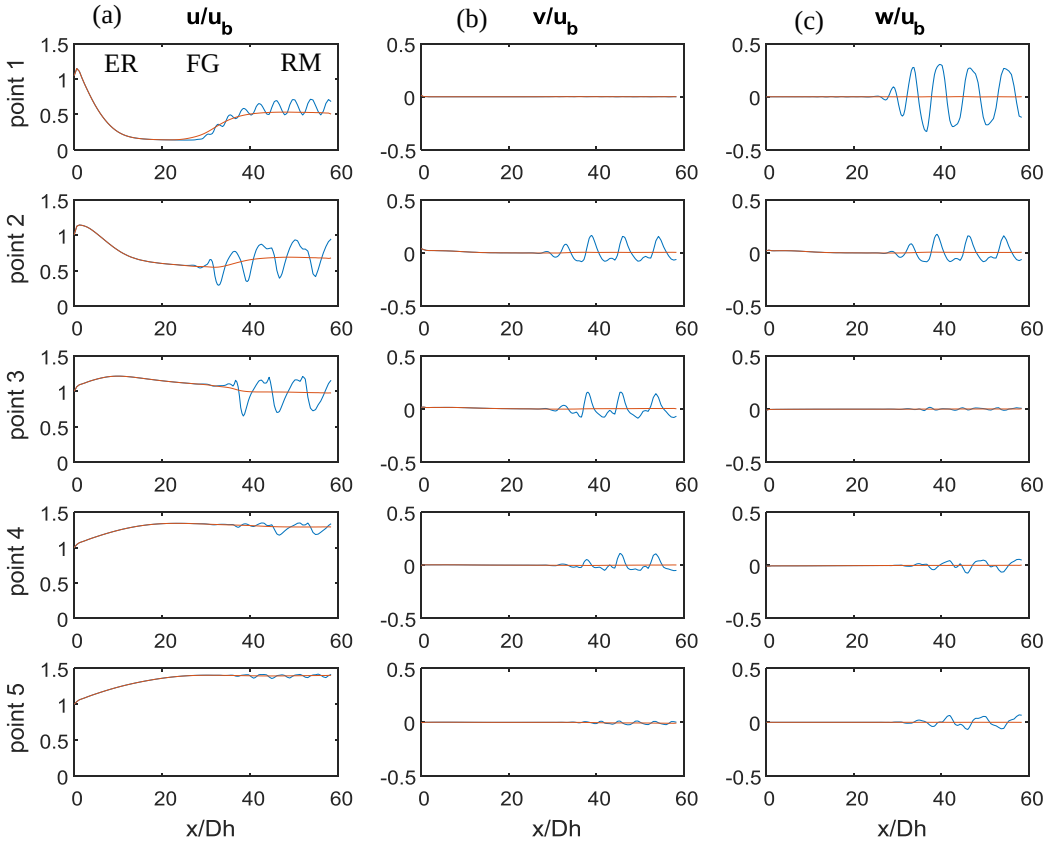

Figure 3. Velocity fluctuations of the three main components at five measurement points for the eccentric case, the blue line represents the fluctuations along the channel and the red line represent the mean of these fluctuations. (a) Stream-wise fluctuations. (b) velocity fluctuations in the v direction. (c) Span-wise fluctuation at the measurement points.

The Figure 4 presents the behavior of the three velocity components for the concentric case, as it is possible to see, this case does not present important velocity fluctuations and the graph shows a line with a behavior that can be compared with the one presented by the wide gap represented by the point five in Fig.3 where the streamwise velocity starts increasing until reach its stable value and the other components remain in 0.

3.2 Convection velocity

For the convection velocity, in FG and RM regions were taken measurements of four points separated 10 *mm* each one in order to make the cross correlation of each region and obtain the frequency who moves the vortex. The convection velocity is obtained by de Eq. (13), the value of λ corresponds to the distance between the peaks of two velocity signals. Figure 4 presents the autocorrelation and cross correlation of the velocity signals in the streamwise direction on the FG region for the eccentric case. The table 2 present the values of convection velocity for the concentric and eccentric case in the three regions. The convection velocity was found to be constant in the FG and RM regions with a value of $\mathbf{0.68}\boldsymbol{U_b}$ for the eccentric case and presented a good agreement with the value presented by Choueiri (Choueiri and Tavoularis, 2014). of $\mathbf{0.65}\boldsymbol{U_b}$. For the concentric case, the convection velocity presented a value of $\mathbf{0.85}\boldsymbol{U_b}$.

$$U_c = \lambda * freq \tag{13}$$

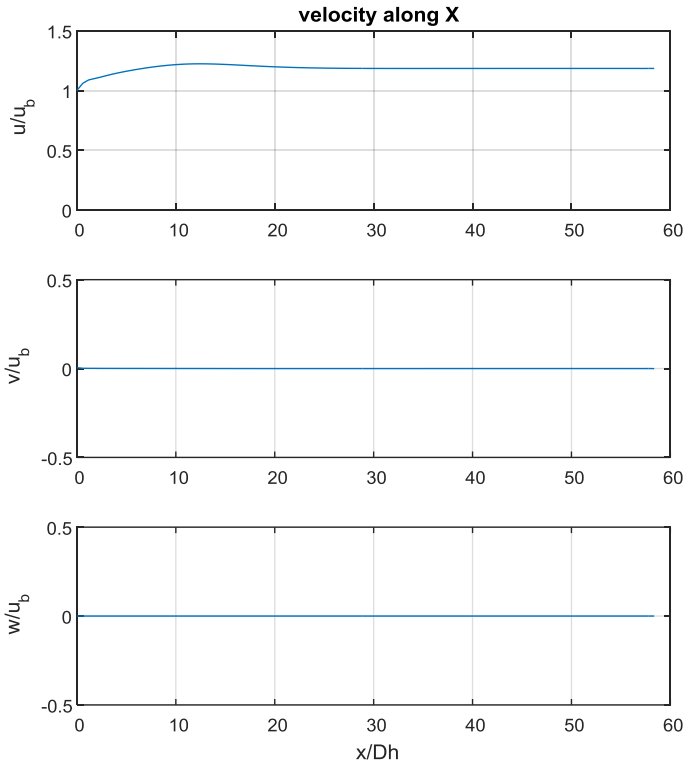

Figure 3. Velocity fluctuations of the three main components for the concentric case

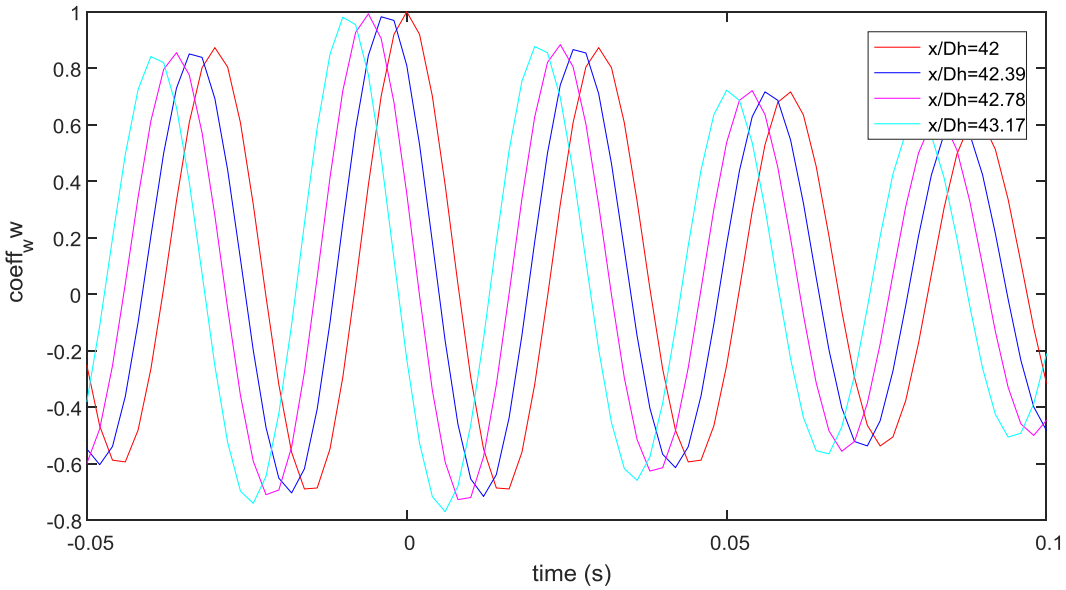

Figure 4. Auto-correlation and cross-correlation coefficients for streamwise velocity for the eccentric case

Table 2. Convection velocities in concentric and eccentric cases

	Convection velocity [m/s]	
Region	*Eccentric case*	*Concentric case*
FG	3	3.7
RM	3	3.75

3.3 Heat Transfer

As it was mentioned before, in order to have a source of comparison and validation for the eccentric case with heat transfer, it was also simulated a concentric case with the same geometry, dynamic characteristics and thermal boundary conditions. The concentric case was validated with the analytical equations given by Gnielinski (2011) that allow to have direct results of friction factor and Nusselt number (*Nu)* having into account the diameter ratio, Reynolds number and the heat transfer conditions. The Equations (14) to (15) presents the correlations used to calculate the friction factor for an annular case.

$$\boldsymbol{f_{ann} = (1.8 \log_{10} Re^{*} - 1.5)^{-2}} \tag{14}$$

$$\boldsymbol{Re^{*} = Re \frac{(1 + a^{2}) \ln a + (1 - a^{2})}{(1 - a)^{2} \ln a}} \tag{15}$$

$$\boldsymbol{a = (D_i / D_o)} \tag{16}$$

Equations (17) to (20) presents the correlations used to obtain the Nusselt number for an annular case, as it is possible to see in the Eq. (17) the Nusselt number depends of other parameter besides the well-known, Reynolds number, Prandtl and friction factor, such as the variation of fluid properties *K* presented in Eq. (18) for the case of heating gas, the factor $\boldsymbol{k_1}$ and the factor *F* that differs if the thermal condition is heat transfer at the inner wall and the outer wall insulated or vice versa. The Equation (20) gives the relation of the *F* factor for the case analyzed in the present work.

$$\boldsymbol{Nu = \frac{(f_{ann}/8) * Re * Pr}{k_1 + 12.7\sqrt{f_{ann}/8} * (Pr^{2}/_{3} - 1)} \left[1 + \left(\frac{D_h}{L}\right)^{2/3}\right] * F_{ann} * K} \tag{17}$$

$$\boldsymbol{K = \left(\frac{T_b}{T_w}\right)^{n} \qquad n = 0.45} \tag{18}$$

$$\boldsymbol{k_1 = 1.07 + \frac{900}{Re} - \frac{0.63}{(1 + 10Pr)}} \tag{19}$$

$$\boldsymbol{F_{ann} = (0.9 - 0.15 a^{0.6})} \tag{20}$$

Figure 5 presents the behavior of the bulk temperature and the wall temperature for the concentric case, it is important to say that for the case “constant heat flux” the completely developed condition is that the difference between the bulk temperature and surface temperature is constant along the streamwise direction. Figure 5 shows an agreement with this definition and lets conclude that the results obtained for the concentric case are in fully developed regime for both dynamic and thermal boundary layers.

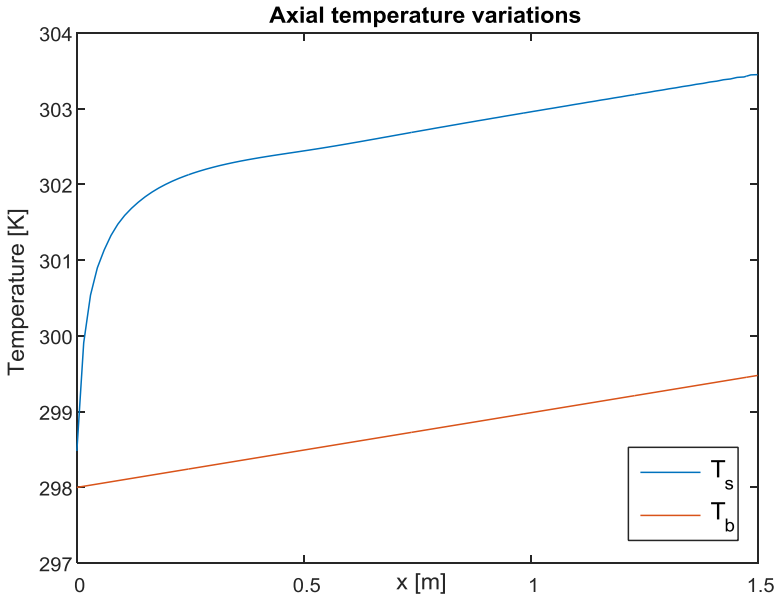

Figure 5. Axial temperature variations for the concentric case

For the calculation of the heat transfer coefficient (*h)* and the Nusselt number in the numeric case the Eq. (21) to (23) given by Incropera (Incropera *et al.* 2008) in their book of fundamentals of heat and mass transfer. Equation (21) presents the relation for the calculation of the mean temperature along the streamwise direction for a case with constant heat flux, with *P* as the perimeter of the surface that is transferring the heat. Equations (22) and (23) presents the relations to obtain the heat transfer coefficient and the Nusselt number respectively.

$$T_m(x) = T_{m,in} + \frac{q_s'' * P}{\dot{m} * C_p} x \tag{21}$$

$$h = \frac{q_s''}{(T_s - T_m)} \tag{22}$$

$$Nu = \frac{h * D_h}{k} \qquad k = Thermal\ conductivity \tag{23}$$

Table 3 presents the results of the friction factor and Nusselt number for the concentric case obtained appliying the Eqs. (14) to (20) and the numeric simulation. It is possible to see that the diference between the simulated and calculated values is really small, this results shows that the methodology, mesh and turbulence models used for the numeric simulations leads to heat transfer coefficients and Nusselts numbers that are in good agreement with the values that can be found in the reality.

Table 3. Numeric and analytic results for heat transfer in a concentric channel

	Numeric Simulation	*Analytic Equations*
Frition factor	0.039	0.036
Nusselt number	24.76	25.27

With the methodology for the numerical simulations validated for the case with heat transfer, the same boundary conditions were applied for the concentric channel. From the Fig. 3 it is possible to see that the point 1 corresponding to the narrow gap is the great interest since it is in that place where the biggest velocity fluctuations appear. As in the Fig. 5, the Fig. 6 presents the temperature variations along the streamwise direction for the transversal section of the channel and the narrow gap region. In both cases, the completely developed region starts around *x/Dh=40*. From this point, the difference between the bulk temperature and surface temperature remain constant with *x*.

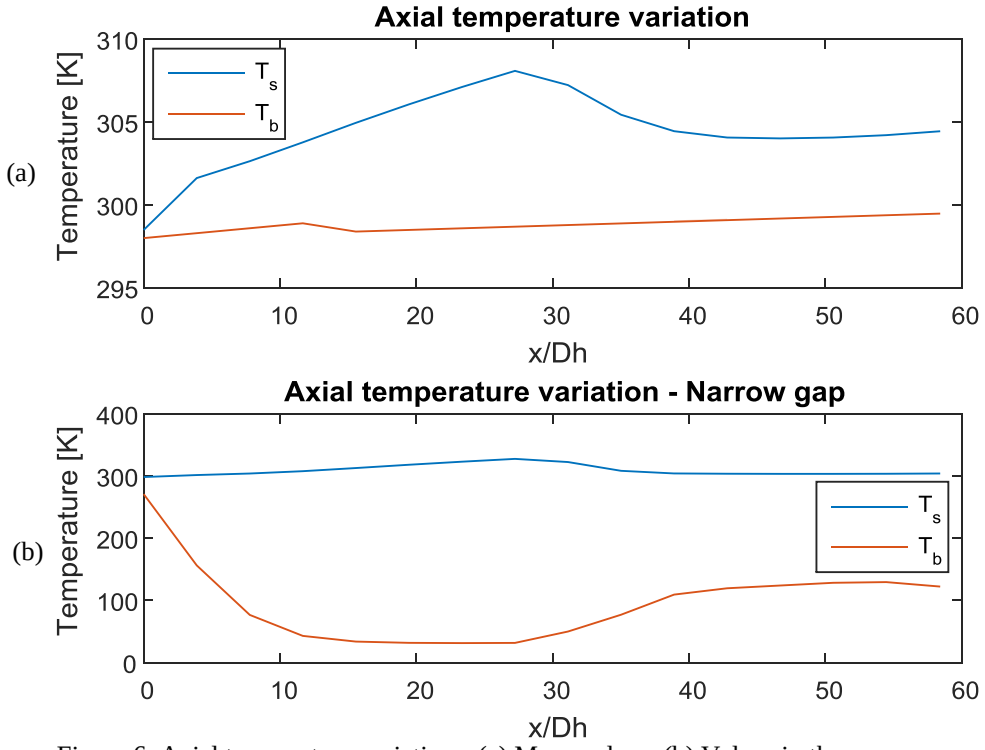

Figure 6. Axial temperature variations. (a) Mean values. (b) Values in the narrow gap.

For the calculation of the local Nussel number the Eq. (24) that describes the bulk temperature in a two dimensional channel was implemented looking for a representing value of the bulk temperature in an specific gap position. The value *2H* in Eq. (24) represents the size of the gap (Narasimhan *et al.*,2001). The variation of the Nusselt number in the eccentric channel and in the narrow gap is presented in Fig. 7. In both cases, the same behavior is shown, although with different magnitudes, This figure allows to find two patterns related to Fig. 3. Figure 7(a) shows the total Nusselt number along *x* that is calculated with all the temperatures and therefore all the fluctuations velocities in each tranversal plane along the streamwise direction and the Fig. 7 (b) presents the local Nusselt number calculated just with the variations in the narrow gap. From Fig.3 was remarkable that in the point 1 the velocity was always lower that in the other measurement points, and knowing that the heat transfer coefficient is dependent of the velocity, a Nusselt number considerably low is expected in the narrow gap, which agrees with the results obtained.

$$T_b(x) = \frac{1}{2HU}\int_0^{2H} (uT)_x dy \tag{24}$$

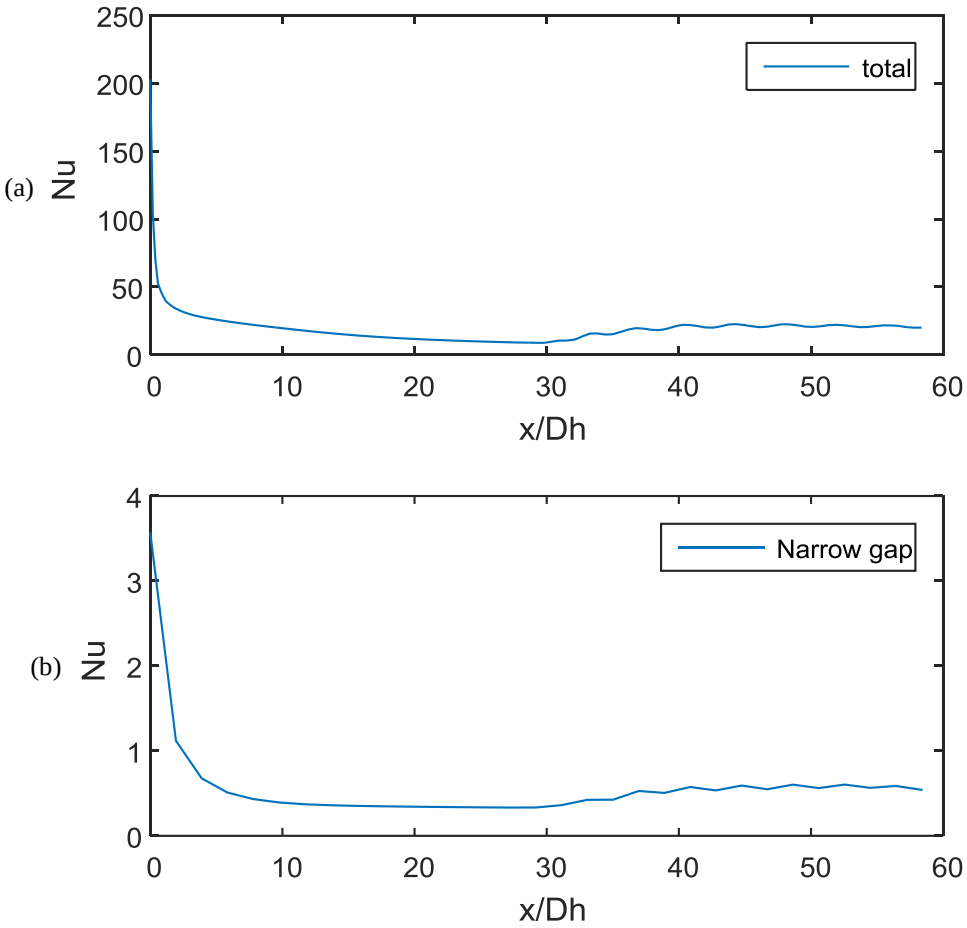

Figure 6. Nusselt number along the streamwise direction. (a) Total Nusselt number. (b) Local Nusselt number in the narrow gap.

According to Möller (1991) in locations near the narrow gap it is possible to find some characteristics of the velocity fluctuation in the streamwise direction that cannot be found easily in the middle of the narrow gap. Taking into account this, the Fig. 8 presents the local Nusselt number for points located at 5º, 10º and 15º measured from the middle of the narrow gap to the middle of the wider gap, each degree was also measured in the regions named in Fig. 3, entrance region, fluctuations growth and rapid mixing.

Knowing from the first section of the present work that the velocity fluctuations start around *x/Dh=30* it is easy to think that the Nusselt number in the FG region would be bigger than in the ER region. In Fig. 9 it is noted that although in effect, in the FG region there are velocity fluctuations more projected, the mean of these fluctuations in all the three degrees is smaller than the mean of the velocity fluctuations in the ER region.

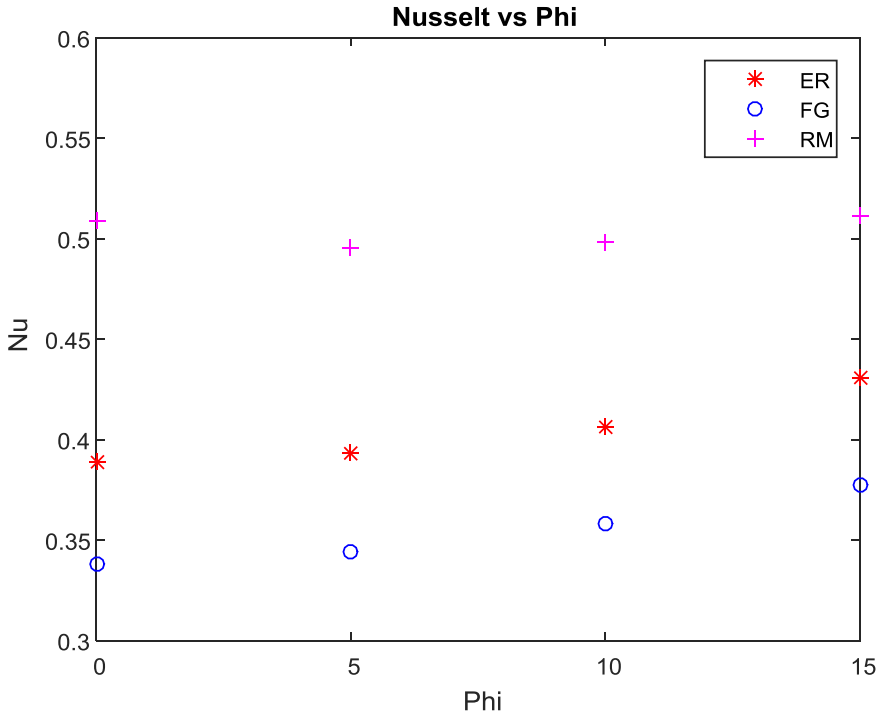

Figure 8. Local Nusselt number near the narrow gap.

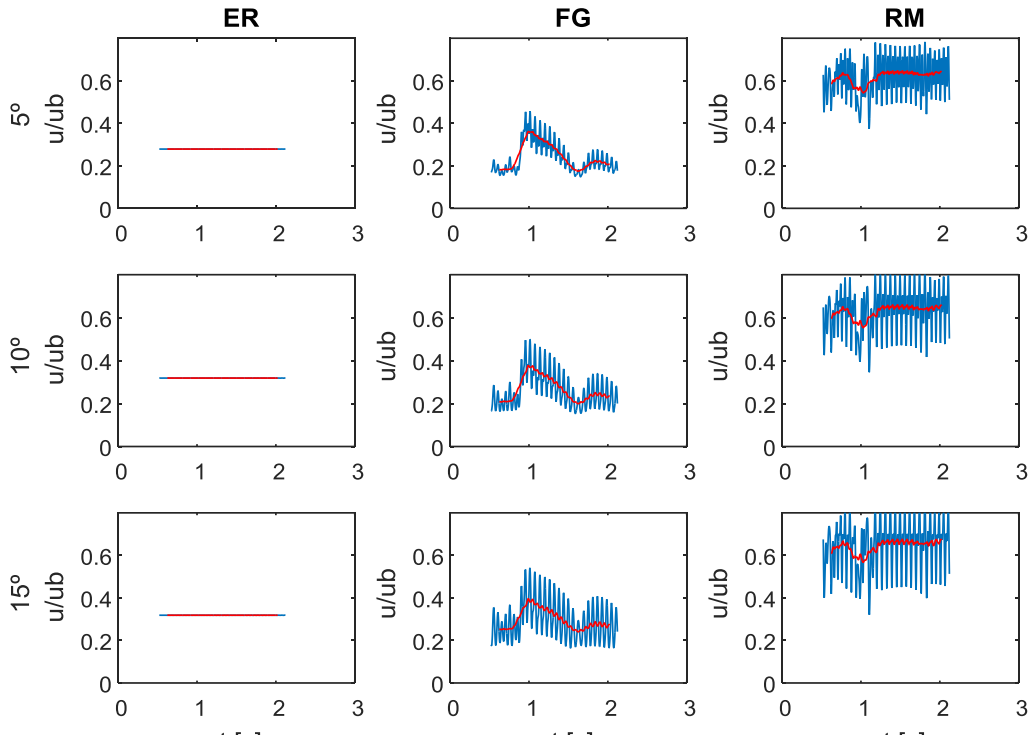

Figure 9. Velocity fluctuations near the narrow gap.

4. CONCLUSIONS

A three dimensional simulation of an eccentric channel with an eccentricity of 0.8, Reynolds number of 7300 an a constant wall heat flux of 100 [W/m^2] was carried out with the software ANSYS-CFX applying an hybrid model DES-SST. A concentric case was also simulated looking for a source of comparison and validation of the heat transfer in the eccentric case along with the work developed by Choueiri (Choueiri and Tavoularis, 2014).

Besides the verification of the dynamical behavior of the flow with the experimental results of Choueiri and Tavoularis (2014) was possible to compare the patterns obtained in the eccentric case with the concentric case. For the velocity fluctuations in the streamwise direction it was found that the concentric case present a behavior that matches

with the one found in the points 3 and 4 of the eccentric case which have a comparable gap size. In this points, the velocity starts with a small increase and rapidly reach its stable value slightly higher than the inlet velocity. It was also noticeable that the convection velocity does not appear to be influenced by the eccentricity maintaining a value almost equal in both cases.

Unlike the convection velocity, the friction factor and the Nusselt number are affected by the eccentricity of the channel, the results found in this work are in agreement with different numerical and experimental works where were found that increasing eccentricity leads to a decrease in the friction factor and Nusselt number compared with the concentric case. (Deissler *et al.*, 1955; Kays *et al.*,1963; Judd *et al.*, 1963; Ogino *et al.*, 1987).

5. REFERENCES

Choueiri, G. and Tavoularis, S., "Experimental investigation of flow development and gap v vortex street in an eccentric annular channel. Part 1. Overview of the flow structure," *J. Fluid Mech,* vol 752, pp. 521-542, 2004.

Dreissler, R. and Taylor, M., "Analysis of fully developed turbulent heat transfer and flow in an annulus with various eccentricities," *National advisory committee for aeronautics-technical note 3451,* 1955.

Djezzar, A.; Chaker, A. and Daguenet, M., "Numerical study of bidimensional steady natural convection in a space annulus between two elliptic confocal ducts," *Influ. Intern. Eccentricity,* vol 8, pp. 63-72, 2005.

Gnielinski, V., "Heat transfer coefficients for turbulent flow in concentric annular ducts*," Heat transfer engineering*, vol. 30, no. 6, pp. 431-436, 2009.

Incropera, F. *et al., Fundamentals of heat and mass transfer*. John Wiley & Sons, New Jersey, 6th edition.

Judd, R. and Wade, J., ., "Forced convection heat transfer in eccentric annular passages,"*Heat transfer and Fluids mechanics Institute,* pp 272-288, 1963.

Kassem, T. "Numerical study of the natural convection process in the parabolic-cylindrical sollar collector,"*Desalination 209,* vol (1-3), pp 144-150, 2007.

Kays, W. and Leung, E., "Heat transfer in annular pasagges-hydrodinamically developed turbulent flow with arbitrary prescribed heat flux," *Int. J. Heat Mass Transfer,* vol 6, pp. 537-557, 1963.

Kuehn, T. and Goldstein, R. "An experimental study of natural convection heat transfer in concentric and eccentric horizontal cylindrical annuly," *J. Heat. Transf.* vol 4, pp 635-640, 1978.

Möller, S., "On phenomena of turbulent flow through rod bundles," *Experimental Thermal and Fluid Science,* vol 4, pp. 25-35, 1991.

Narasimhan, A.; Lage, J. and Nield, D., "New theory for forced convection trhough porous media by fluids with temperature-dependent viscosity," *Journal of Heat Transfer,* vol. 123, pp. 1045-1051, 2001.

Ogino, F.; Sakano, T. and Mizushina, T., "Momentum and heat transfers from fully developed turbulent flow in eccentric annulis to inner and outer tube walls," *Warme und Stoffubertragung,* vol. 21, pp. 87-93, 1987.

Reynolds, W.; Lundberg, R. and McCuen, P., "Heat transfer in annular passages," *Int J Heat Mass Trans,* vol 6, pp. 483–529, 1963.

Strelets, M., "Detached eddy simulation of massively separated flows," *39th Aerospace sciences meetin and exhibit*, 2001.

Teamah, M.; Sorour, M. and Saleh, R., "Mixed convection between two horizontal concentric cylinders when the cooled outer cylinder is rotating," *Alex. Eng. J.,* vol. 3, pp. 347-360, 2000.

6. RESPONSIBILITY NOTICE

The authors are the only responsible for the printed material included in this paper.